

Rapid Monitoring of the Nature and Interconversion of Supported Catalyst Phases and of Their Influence upon Performance: CO Oxidation to CO₂ by γ -Al₂O₃ Supported Rh Catalysts

Mark A. Newton,^{*,[c]} Andrew J. Dent,^[b] Sofia Diaz-Moreno,^[b] Steven G. Fiddy,^[d] Bhrat Jyoti,^[a] and John Evans^{*,[a, b]}

Abstract: Spatially and temporally resolved energy-dispersive EXAFS (EDE) has been utilised in situ to study supported Rh nanoparticles during CO oxidation by O₂ under plug-flow conditions. Three distinct phases of Rh supported upon Al₂O₃ were identified by using EDE at the Rh K-edge during CO oxidation. Their presence and interconversion are related to the efficiency of the catalysts in oxidising CO to CO₂. A metallic phase is

only found at higher temperatures (>450 K) and CO fractions (CO/O₂ > 1); an oxidic phase resembling Rh₂O₃ dominates the active catalyst under oxygen-rich conditions. Below about 573 K, and in CO-rich environments, high proportions of isolated Rh^I(CO)₂

Keywords: EXAFS spectroscopy • heterogeneous catalysis • micro-reactors • oxidation • rhodium

species are found to co-exist with metallic Rh nanoparticles. Alongside these discrete situations a large proportion of the active phase space comprises small Rh cores surrounded by layers of active oxide. Confinement of Rh to nanoscale domains induces structural lability that influences catalytic behaviour. For CO oxidation over Rh/Al₂O₃ there are two redox phase equilibria alongside the chemistry of CO and O adsorbed upon extended Rh surfaces.

Introduction

The behaviour of supported phases used to catalyse commercially important chemical conversions has been widely studied. These complex systems are defined by a multi-dimensional parameter space that includes variables such as temperature, feedstock composition, contact time, particle

size (dispersion), conversion, and selectivity. As such, a complete picture of how such materials behave as they do requires wide-ranging investigations exploring and deconstructing this parameter space. A varied array of approaches has been deployed toward this end each of which has its relative strengths and weaknesses. For instance, a large body of research using planar single-crystal Rh or polycrystalline Rh substrates prepared under ultra high vacuum (UHV) conditions has been used to build up models of the reactivity of highly dispersed systems.^[1–15] Such studies are imbued with a high degree of control of the surfaces under study and therefore considerable molecular and kinetic specificity. As such they have been widely applied to one of the (notionally) simplest conversions in catalysis, CO oxidation to CO₂ by O₂. These studies are based upon the axiom that a quasi-infinite, and therefore low dispersion, metal surface represents a reasonable model of what may be highly dispersed nanoparticles. Nevertheless, some previous studies utilising elevated pressure surface science measurements on Rh single crystals have reported close kinetic correlations between such measurements and the performance of high area catalysts for CO oxidation;^[7,8] these studies have reported this reaction to be essentially insensitive to surface structure at high surface coverage of CO and low temperature. Structure

[a] B. Jyoti, Prof. J. Evans
School of Chemistry, University of Southampton
Southampton, SO17 1BJ (UK)
Fax: (+44)2380-593-781
E-mail: je@soton.ac.uk
john.evans@diamond.ac.uk

[b] Dr. A. J. Dent, S. Diaz-Moreno, Prof. J. Evans
Diamond Light Source, Chilton, Oxfordshire OX11 0QX (UK)
Fax: (+44)1235-778-499

[c] Dr. M. A. Newton
The European Synchrotron Radiation Facility
Grenoble, 38043 (France)
Fax: (+33)476-882.020
E-mail: newton@esrf.fr

[d] Dr. S. G. Fiddy
CLRC Daresbury Laboratory
Warrington, WA4 4 AD (UK)

sensitivities have been observed especially when the surface coverage of adsorbed oxygen becomes appreciable.^[14] By contrast, clear deficiencies in the extrapolation of data from Rh single crystals to that derived from high area systems in the more complex, and structure-sensitive, catalytic reduction of NO by CO have also been reported.^[7,8,16,17]

Through the application of EDE (energy-dispersive EXAFS) to the study of highly dispersed Rh catalysts toward NO, we have shown that Rh nanoparticles may be very rapidly oxidised through the dissociative adsorption of NO at room temperature.^[18] Further, in the case of NO reduction by H₂, practically all the unwanted production of N₂O is due to the presence of an oxidised phase and/or its reductive collapse to form metallic Rh nanoparticles.^[19] In the case of CO oxidation, other studies based upon high area systems have also indicated that the behaviour of a highly dispersed Rh catalyst is more complex than the Rh single crystal limit would indicate. At least eight discrete forms of adsorbed CO have been identified on supported Rh/Al₂O₃ systems under differing conditions, with only a fraction clearly associated with metallic Rh surfaces.^[20] One of these non-metallic species has been long known to result from the lability of very small Rh nanoparticles in the presence of CO, leading to the formation of isolated Rh^I(CO)₂ species.^[20–31] Fourier transform infrared studies have shown that this species may be formed during CO oxidation but that it takes no part in the catalytic conversion.^[29–31] Further, frequency modulation techniques combined with IR^[31] have postulated that the active CO species present is associated with Rh in a +1 oxidation state.

Ex situ XPS studies have also demonstrated the coexistence of highly oxidised and reduced forms of supported

rhodium at elevated temperature (573 K).^[32] These studies have been augmented by scanning EXAFS experiments which have shown that small Rh particles can oxidise at room temperature.^[33,34] In contrast, Rh single crystals are only observed to oxidise extensively at temperatures in excess of 500 K and in extremely lean environments (O₂/CO > 30).^[2,3]

In comparison with scanning EXAFS experiments, the use of a bent monochromator in EDE has two desirable ramifications.^[35] The first of these is that an entire EXAFS spectrum may be acquired instantaneously; this leads to the well known capacity for EDE to yield a higher (ca. <1 s) time resolution together with the local structure determination inherent to the EXAFS experiment. The second ramification is a tightly focused X-ray beam that may be <50 μm horizontally and ~200 μm vertically. This property renders EDE a spatial, as well as temporal, probe of local structure. Thus far this second property of the EDE experiment has only been exploited in the study of very high-pressure chemistry.^[36] Here we utilise both of these properties to map out how the structure and activity of supported Rh catalysts varies according to parameters such as feedstock composition, temperature, and axial position along a catalyst bed.

Results

Interaction of Rh nanoparticles with O₂: All studies were carried out on a non-porous alumina on a bed of powdered catalyst to minimise intra- and inter-particle diffusion constraints. Figure 1a shows Rh K-edge absorption spectra derived from a “fresh” 5 wt %, γ-Al₂O₃ supported Rh sample,

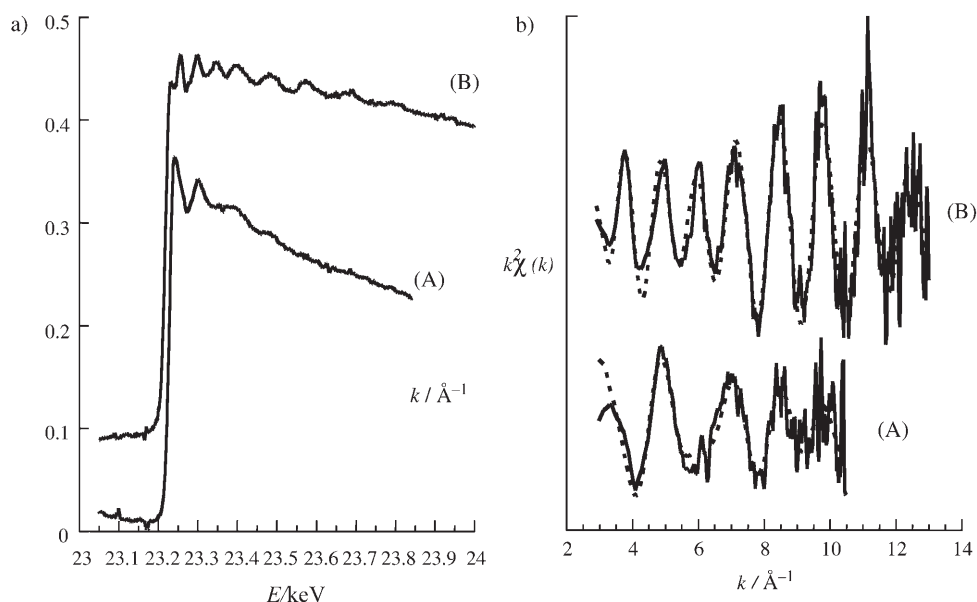


Figure 1. a) Energy-dispersive X-ray absorption spectra derived from (A) a “fresh” 5 wt % Rh, γ -Al₂O₃ sample maintained under He purge at room temperature, and (B) that derived from the same sample after a brief exposure to a 10 mL min⁻¹, 5 % H₂/He flow (also at room temperature). b) k^2 -weighted EXAFS (solid lines) derived from (A) a “fresh” 5 wt % Rh, γ -Al₂O₃ sample maintained under He purge at room temperature, and (B) that derived from the same sample after a brief exposure to a 10 mL min⁻¹, 5 % H₂/He flow (also at room temperature). Theoretical fits (dashed lines) from spherical wave analysis in EXCURV98 are also shown.

Table 1. Local order and statistical parameters derived from the analysis in EXCURV98 of the EDE spectra derived from the fresh, and room-temperature re-reduced samples shown in Figure 1 a and 1 b.

Spectrum	Time/spectrum ^[a]	k_{\min} [Å ⁻¹]	k_{\max} [Å ⁻¹]	Shell	CN ^[b]	$r^{[c]}$ [Å]	$2\sigma^2$ [Å ²]	E_F	R [%]
A - "fresh"	400 ms	3	10.5	Rh O	2.0(2) 3.0(3)	2.67(4) 2.00(2)	0.009(2) 0.011(2)	-3.4	55
B -post 4% H ₂ /He@300 K	400 ms	3	13	Rh	7.3(6)	2.65(2)	0.011(1)	-8.6	45

[a] Total time/spectrum = Number of detector strips (10) × number of acquisitions (10) × accumulation time per strip. [b] CN = Co-ordination number; errors should be considered to be about ±20% for spectrum A and about ±15% for spectrum B. [c] Realistic errors in bond length determination should be considered to be about 1.5–2%. Values in parentheses are statistical errors generated in EXCURV98. Other parameters: AFAC=1; VPI=0.

maintained under a He flow (A) and after brief exposure to 5% H₂/He at room temperature (B). Figure 1 b shows the k^2 -weighted EDE of these spectra with theoretical fits obtained in EXCURV98. The results derived from analysis of these data are collated in Table 1. It is clear that the EDE derived from the "fresh" Rh/Al₂O₃ sample maintained under He is not that of particulate Rh. The Rh component of the sample is instead clearly oxidised ($N_1^{Rh} \sim 2$, $N_2^O \sim 3$) after exposure to air at room temperature, consistent with the scanning EXAFS results reported by Martens et al.^[33,34] In the raw adsorption data (Figure 1) the prominent absorption structure in the near-edge region is also indicative of Rh in oxidation state +III. Brief exposure to H₂ results in more extensive EXAFS oscillations characteristic of a metallic Rh environment, with a concomitant and distinctive change in near-edge structure.

Figure 2 shows phase-corrected Fourier transforms derived from EDE measurements made on a sample reduced as for Figure 1 (spectrum B) during the exposure to 5% O₂/

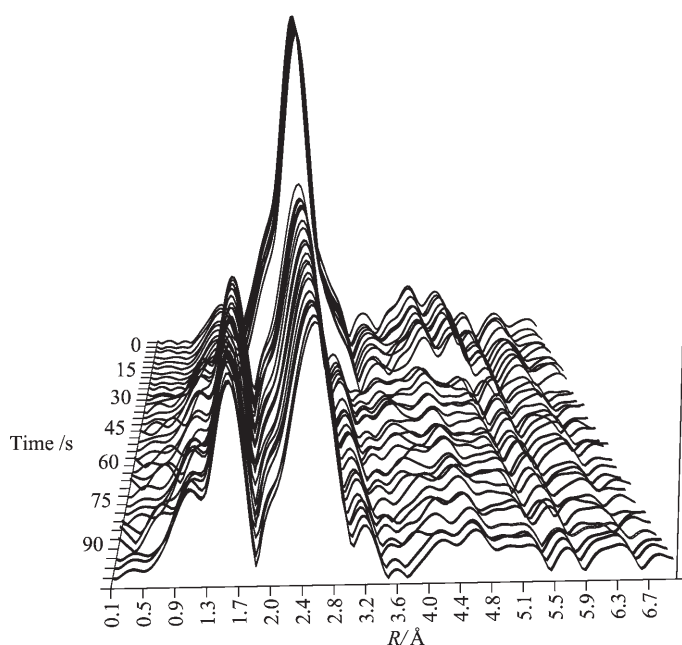


Figure 2. Variation in phase-corrected Fourier transforms derived from energy-dispersive X-ray absorption spectra obtained during the exposure of a reduced 5 wt % Rh/γ-Al₂O₃ sample to 10 mL min⁻¹ 5% O₂/He flow at room temperature. Acquisition time per spectrum = 600 ms; sequential spectral acquisition rate about 0.2 Hz.

He at room temperature; this gives a clear indication of rapid structural changes occurring with the gas switch (at $t \sim 30$ s). A major loss of first shell Rh–Rh co-ordination occurs between scans, which were acquired at 0.3 Hz. This is accompanied by a total attenuation of contributions of Rh··Rh shells (between 4 and 5.5 Å) and the evolution of a shell attributable to Rh–O. After this step, the residual first shell Rh–Rh co-ordination number is continues to attenuate, but at a considerably slower rate.

Figure 3 presents representative k^3 -weighted EXAFS data derived in such experiments, and Table 2 summarises the

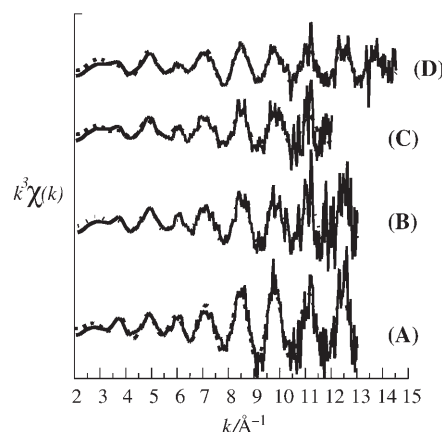


Figure 3. k^3 -weighted EDE spectra (solid lines), along with theoretical fits (dashed lines) derived from spherical wave analysis in EXCURV98: Spectral labels A–C refer to differing temporal positions within the gas switching experiment shown graphically in Figure 4a. Spectrum D was taken about 1000 s after the switch to a 5% O₂/He feed. Spectra A–C have a total acquisition time of 45 ms; spectrum D with 900 ms.

local order and statistical data produced by analysis in EXCURV98. Figure 4a shows results of EXAFS analysis for Rh–Rh co-ordination (N_1^{Rh}); the labels (A–C) refer to the k^3 -weighted spectra shown in Figure 3. Figure 4a was derived with an EDE sampling rate of about 18 spectra per minute (450 ms spectral acquisition time); the insert in Figure 4a shows in more detail the major transition region with a spectral sampling rate of about 92 spectra per minute (45 ms spectral acquisition time). O₂ uptake and the variation in sample bed temperature (Figure 4b) occur simultaneously with the structural changes.

Table 2. Local order and statistical parameters derived from the analysis in EXCURV98 of the EDE spectra derived from the fresh, and room temperature re-reduced samples shown in Figure 3.

Spectrum	Time/spectrum ^[a]	k_{\min} [Å ⁻¹]	k_{\max} [Å ⁻¹]	Shell	CN ^[b]	$r^{[c]}$ [Å]	$2\sigma^2$ [Å ²]	E_F	R [%]
A -post 4% H ₂ /He@300 K	450 ms	2	13	Rh	7.5(6)	2.66(2)	0.011(1)	-7.9	51
B -post 10 s 4% O ₂ /He@300 K	450 ms	2	13	Rh	4.5(5)	2.67(3)	0.01(2)	-6.4	65
				O	2.0(2)	2.04(1)	0.008(2)		
C -post 150 s 4% O ₂ /He@300 K	450 ms	2	12	Rh	3.4(4)	2.66(2)	0.010(2)	-6.8	56
				O	2.0(2)	2.08(2)	0.007(3)		
D - post 1000 s 4% O ₂ /He@300 K	900 ms	2	14	Rh	3.5(3)	2.68(1)	0.010(1)	-4.5	46
				O	2.0(2)	2.02(2)	0.010(2)		

[a] Total time/spectrum = Number of detector strips (10) × number of acquisitions × accumulation time per strip (4.5 ms). [b] CN = Co-ordination number: errors should be considered to be about ±20%. [c] Realistic errors in bond length determination should be considered to be about 1.5–2%. Values in parentheses are statistical errors generated in EXCURV98. Other parameters: AFAC=1; VPI=0.

Thus, the interaction of O₂ with reduced Rh nanoparticles results in very rapid and exothermic oxidation: the average Rh–Rh co-ordination decreases from 7 to 4.5 in less than 5 s. Thereafter a much slower decrease in N_1^{Rh} is indicated; it reaches about 3.5 after 550 s exposure to the 5% O₂/He feedstock. Given that the reduced particles initially present yield an average N_1^{Rh} of 7, and that a fully oxidised Rh₂O₃ displays a Rh–Rh co-ordination of 2, these results suggest that in the first 5 s of O₂ exposure about 50% of the Rh atoms present in the sample are oxidised, this percentage rising to about 70% after 550 s.

In situ examination of the structure and reactivity of Rh samples during CO oxidation: Figure 5 shows the net levels of CO conversion obtained from initially reduced Rh/Al₂O₃

catalysts exposed to a feedstock of varying CO/O₂ ratios at room temperature and then heated at 10 K min⁻¹ to 573 K. Figure 6 shows the corresponding variation in the levels of oxidation of the Rh, derived from the value of N_1^{Rh} calculated from EDE spectra obtained concurrently. Under all feedstock compositions, a high level of CO conversion can be achieved. The temperature at which catalysis is initiated, however, varies considerably, with progressively reducing environments resulting in progressively higher “light off” temperatures. At temperatures below light off the Rh exists in oxidised states irrespective of feedstock composition. In net reducing conditions the onset of catalysis correlates well with the formation of reduced Rh nanoparticles; under CO lean conditions the Rh continues to oxidise as the temperature is increased and this is not deleterious to CO conver-

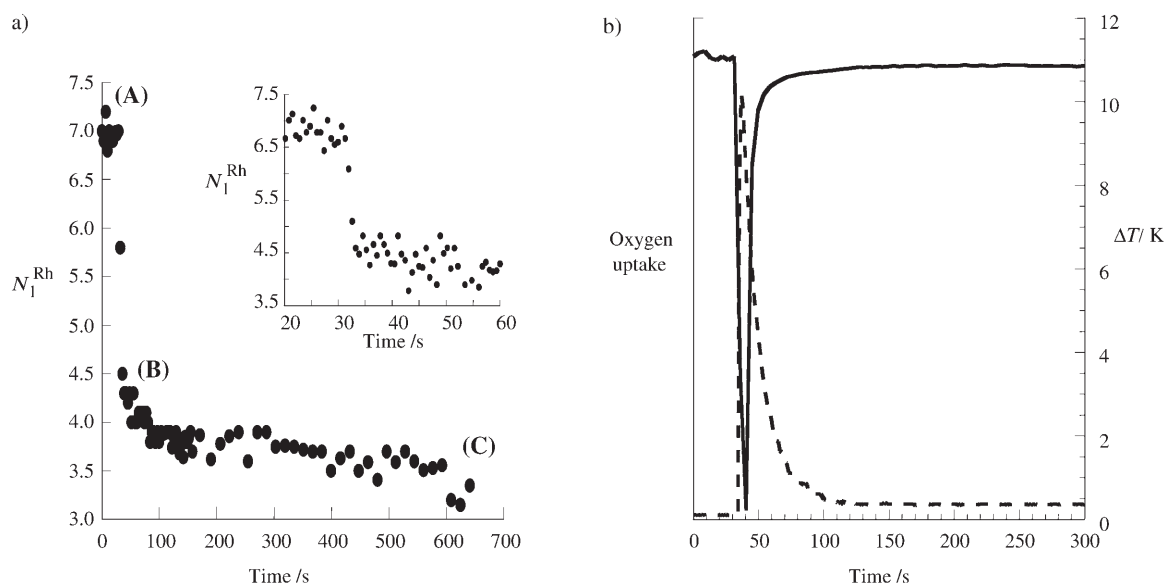


Figure 4. a) Variation in N_1^{Rh} derived from analysis in EXCURV98 of the spectra shown in Figure 3 (acquisition rate ~0.3 Hz), during gas switching (at $t=30$ s) from 10 mL min⁻¹ He, to 10 mL min⁻¹ 5% O₂/He flow at room temperature. The labels A–C refer to the k -weighted spectra shown in Figure 3 A–C. The insert shows the region around the gas switch in more detail from a second run with spectral acquisition rate of about 1.5 Hz. Errors in co-ordination number should be considered to be of the order of ±15–20%. b) Temporal variation in O₂ uptake (mass 32, solid line) during the switch from He to 5% O₂/He at room temperature, along with the observed variation in the temperature (dashed line) of the sample bed.

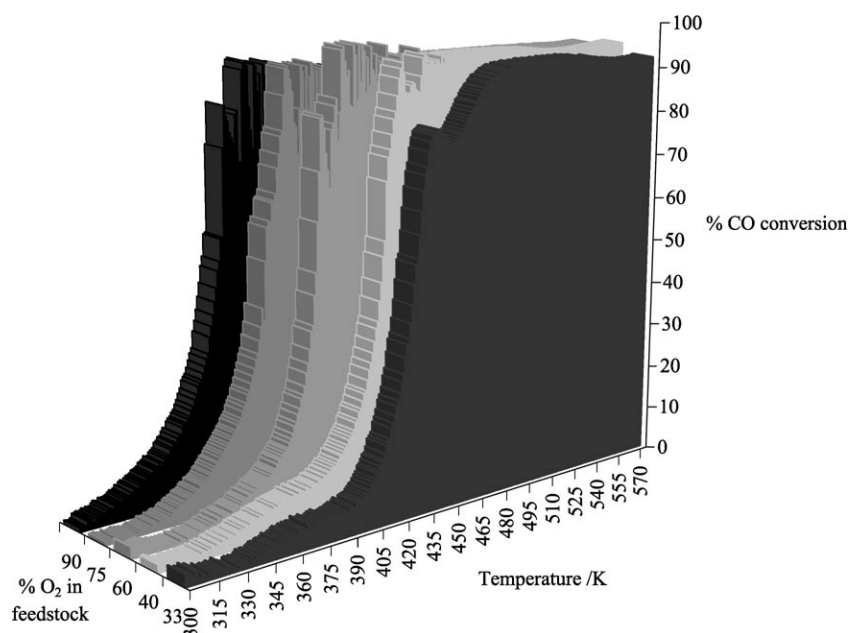


Figure 5. Variation in the observed CO conversion attained over 5 wt% Rh/ γ -Al₂O₃ samples as a function of temperature and feedstock composition during CO oxidation reactions (after subtracting contributions to the mass 28 signal due to the formation of CO₂).

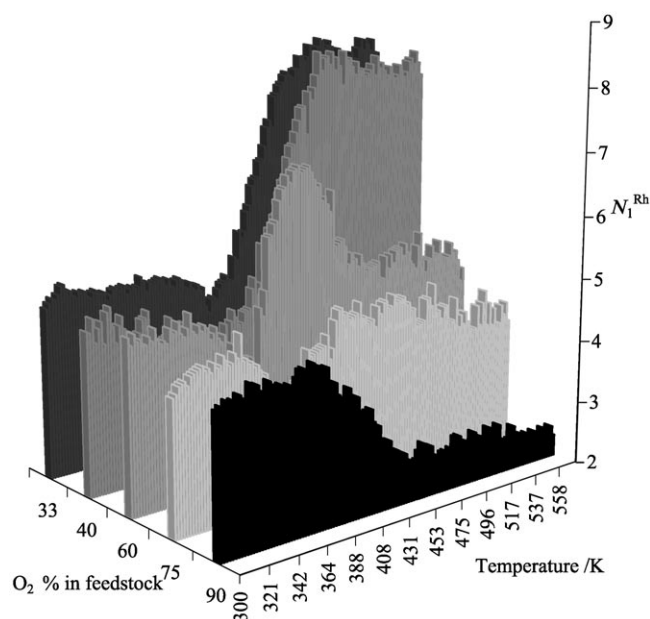


Figure 6. Variation of N_1^{Rh} derived from analysis of EDE as a function of temperature and feedstock composition during CO oxidation reactions. Errors in co-ordination number should be regarded as being of the order of $\pm 20\%$.

sion. Indeed, reaction light off occurs at considerably lower temperatures than in reducing conditions. In between these two extremes of feedstock composition, various intermediate situations are observed with a particularly interesting situation displayed under an equimolar mixture of CO and O₂. In this case a reduced phase develops with increasing tem-

perature, and CO conversion ensues. However, the appearance of a reduced Rh phase is only transient, and it is superseded as the temperature is increased further by a return of the Rh to a state wherein it is approximately 50% oxidised; this change in the active phase structure causes no impediment to CO conversion.

The above indicates firstly that an obviously reduced Rh phase is only produced over a restricted range of feedstock composition and temperatures. Secondly, the rapid mapping of a wide range of this parameter space afforded by EDE/MS indicates that effective CO conversion may be achieved by using Rh in a variety of forms. Importantly in the lean feedstock limit, a Rh phase similar to Rh₂O₃ (vis à vis Figure 1,

Table 1), is a highly effective catalyst and displays the lowest light off temperature.

Spatial mapping of Rh/Al₂O₃ during CO oxidation: The focused nature of the X-ray beam only samples a very small portion of the total catalyst bed. Given the plug flow nature of the microreactor, the structural data derived from the middle of the catalyst bed may not be representative of its entirety. As the composition of the gas phase is changing along the bed under conditions of appreciable conversion, axial phase gradients in the Rh structure may exist.

EDE measurements were then made sequentially from the exhaust end of the bed to the gas inlet end of the bed in 200 μm steps. The temperature was then ramped by 25 K and the process repeated in the range 373 K–573 K, with an example shown in Figure 7. In all these cases, no gross axial variations in local Rh structure exist within this catalyst bed. Structural analysis does show that small variations in the level of oxidation (as derived from N_1^{Rh}) may, however, be detected. In Figure 7c (at 448 K with CO:O₂=0.11 and a CO conversion of 90%), the Rh is more reduced at the reaction inlet end of the bed than at the exit end. At the exit end where the spectra obtained are found to be identical to the Rh^{III} species derived from the fresh samples of Rh/Al₂O₃ (Figure 1). These spectra confirm that the structural correlations derived from the previous experiments (Figure 5 and Figure 6) are indeed broadly valid but also indicate the limitations of such an approach. It is clear that under the most oxidising conditions, and where there is a high level of CO conversion being attained, Rh exists in a state that is essentially oxidic. At the gas inlet end of the bed (within the first 1–2 mm) a partial reduction of the

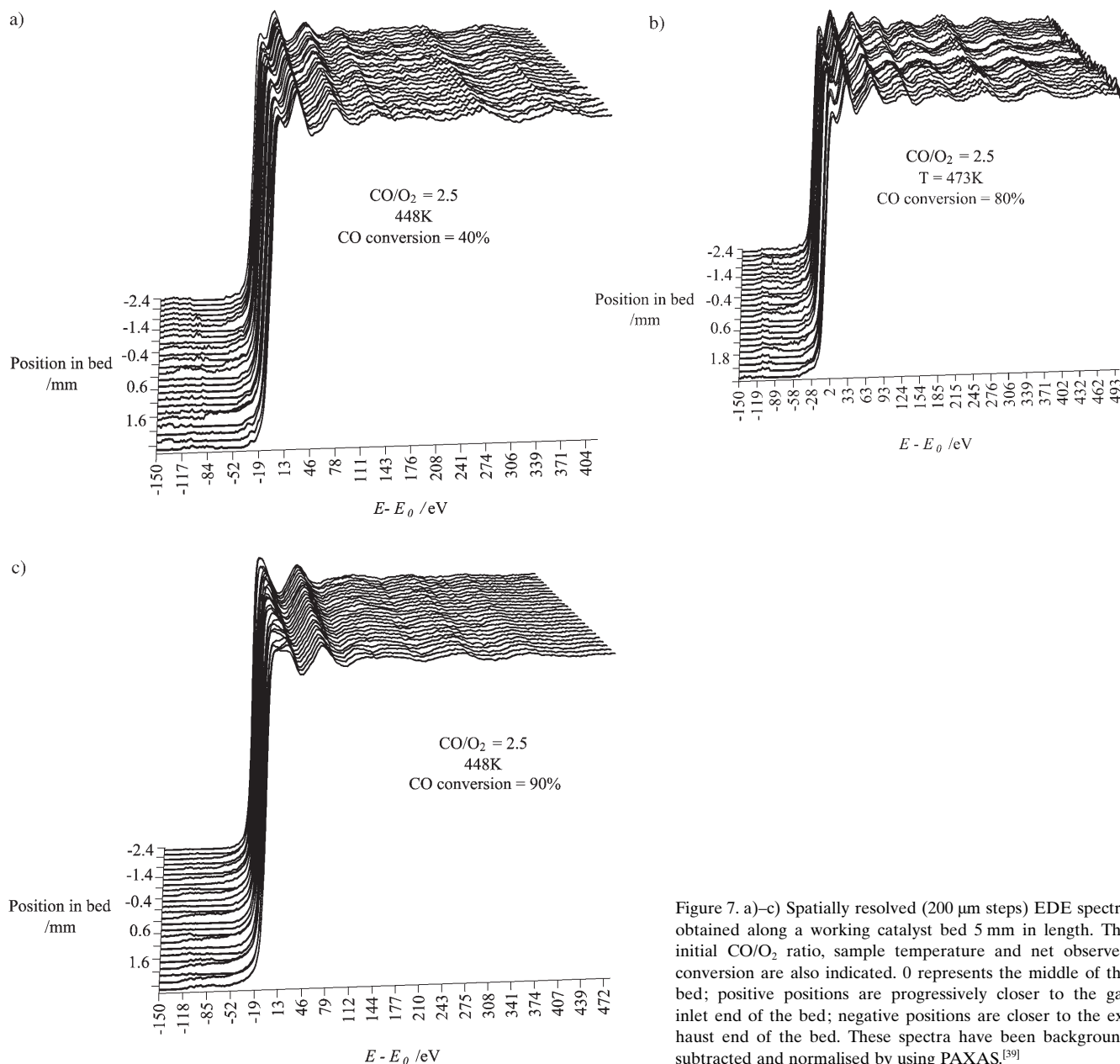


Figure 7. a)–c) Spatially resolved (200 μm steps) EDE spectra obtained along a working catalyst bed 5 mm in length. The initial CO/O_2 ratio, sample temperature and net observed conversion are also indicated. 0 represents the middle of the bed; positive positions are progressively closer to the gas inlet end of the bed; negative positions are closer to the exhaust end of the bed. These spectra have been background subtracted and normalised by using PAXAS.^[39]

oxide (from XANES) is evident, indicating that it is in this portion of the bed where the majority of CO conversion is occurring. Figure 8 shows the results of a component analysis, by spectral additions, of the XAFS at this point in the bed. A linear combination of purely metallic (A) and purely oxidic (B) components (Figure 1) can be used to fit the experimental EXAFS derived at this point in the bed (C) and indicate that the Rh is 70–80% oxidised in the active region of the bed. From Figure 6 we can see that once fully reduced at similar temperatures (though albeit under more reducing conditions) the metallic Rh phase yields a first shell Rh coordination of about eight. This corresponds to an average Rh particle containing about 75 atoms and therefore an average particle diameter of 14–15 Å (assuming a hemispherical morphology).^[41] On the assumption that the distri-

bution of Rh is not grossly altered by the oxidation/reduction of the Rh, the 70–80% of the Rh indicated to be oxidised in Figure 8 implies that the average Rh particle within this active phase comprises a metallic core (~15–22 atoms) surrounded by a Rh oxide phase.

Under reducing conditions ($\text{CO}:\text{O}_2=2.5:1$) these additional spatially resolving experiments again show that our initial survey of the local Rh environment, based solely on an assessment of the apparent Rh–Rh co-ordination, does not fully describe the Rh structures present. There are tangible changes in the EXAFS and XANES patterns. The XANES region clearly indicates that this is not an oxidic (Rh^{III}) form of Rh of the type observed under much leaner feedstocks. The near edge structure and the low-energy EXAFS region are very strikingly similar to that observed

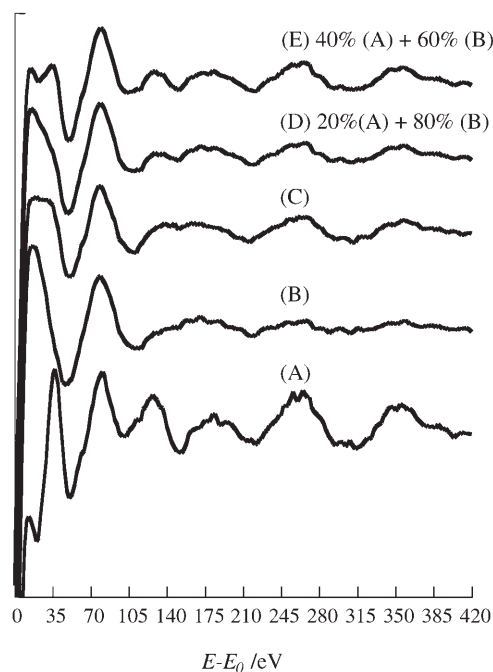


Figure 8. A) Rh K-edge EDE from reduced Rh nanoparticles. B) Rh K-edge EDE from an oxidised Rh sample (from Figure 1). C) Rh K-edge EDE spectrum from Figure 7 at the gas inlet end of the catalyst ($\text{CO}/\text{O}_2=0.11$, $T=448$ K). Spectra D and E result from linear combinations of spectra A and B as indicated.

from 5wt% Rh/ Al_2O_3 derived from the dissociative adsorption of $[\text{Rh}^{\text{I}}(\text{CO})_2\text{Cl}]_2$ over hydroxylated $\gamma\text{-Al}_2\text{O}_3$.^[42,43] This procedure results in the uniform formation of adsorbed $(\text{AlO})\text{Rh}^{\text{I}}(\text{CO})_2\text{Cl}$ species. Figure 9 shows this in more detail by directly comparing the EXAFS derived previously from this $\text{Rh}^{\text{I}}(\text{CO})_2$ species (C) with that obtained from the gas inlet end at 448 K (CO conversion 40%) (A) and also at 473 K (CO conversion 80%) (B). A linear combination approach was applied and the best fit was a composite spectrum comprising 40% (C) convoluted with 60% (B) as shown (D). The insert shows a comparison of k^3 weighted EXAFS derived from the gas inlet at 448 K (A) with that derived from the composite spectrum (D). From both these spectra it is clear that very significant levels of a $\text{Rh}(\text{CO})_2$ species (comprising ca. 40% of the total Rh in the system) co-exist alongside metallic Rh under these reactive conditions at temperatures < 473 K.

Figure 10 shows TEM data derived from the “fresh” 5wt%

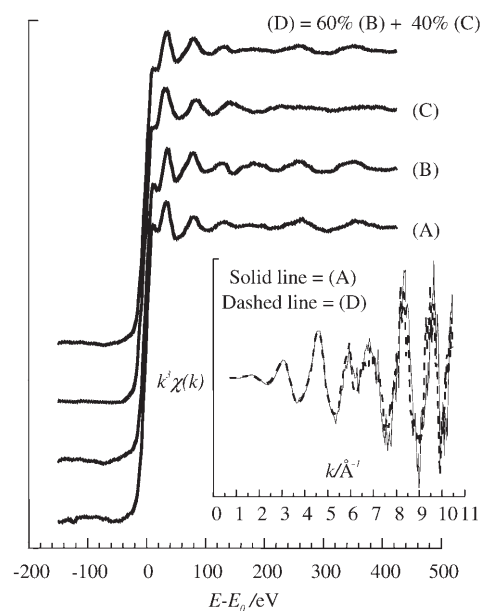


Figure 9. A) Rh K-edge EDE from gas inlet end of the catalyst bed for $\text{CO}/\text{O}_2=2.5$, $T=448$ K). B) Rh K-edge EDE from gas inlet end of the catalysts bed for $\text{CO}/\text{O}_2=2.5$, $T=473$ K). C) Rh K-edge EDE derived from 5 wt% $\text{Rh}(\text{CO})_2\text{Cl}$ adsorbed upon $\gamma\text{-Al}_2\text{O}_3$.^[42,43] D) A composite XAS spectrum derived from 60% spectrum B and 40% spectrum C. The insert shows a comparison of k^3 -weighted spectra derived from A (solid line) and D (dashed line).

Rh samples (A). This yields a mean average particle diameter of 21.5 Å. The XAFS measurements (Figure 1) indicate that such samples are oxidic rather than metallic and therefore this mean particle size refers to that of a Rh_2O_3 -like phase. This is borne out by considering that a hemispherical metallic Rh particle of this size should be expected to yield a Rh–Rh co-ordination of about nine.^[41] Assuming that re-

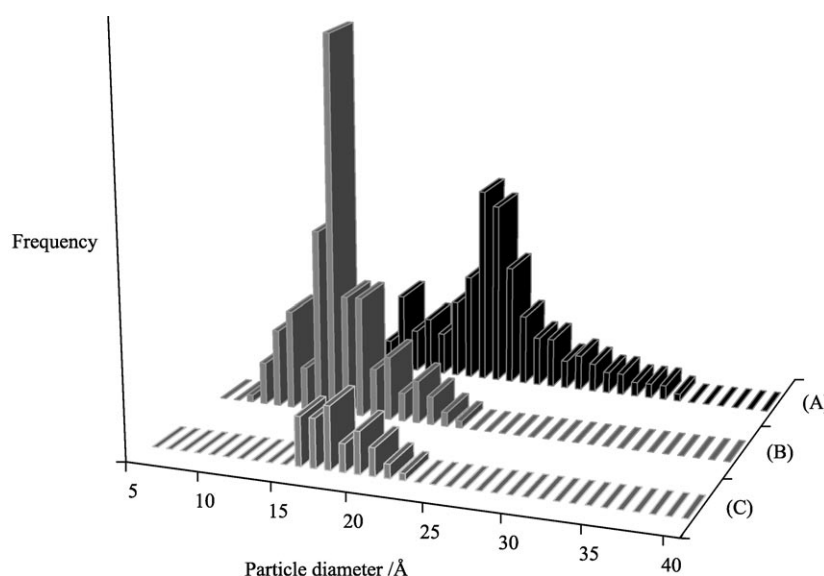


Figure 10. Particle size distributions derived from TEM measurements made upon A) “fresh” and oxidic (vis à vis Figure 1, spectrum A) 5 wt% Rh catalysts; B) that derived from A after accounting for the differing densities of Rh metal and Rh_2O_3 ; and, C) after that portion of the distribution shown in B, comprising 40% of the total Rh content, has been removed.

duction of this phase does not cause a gross redistribution of the Rh, and by taking account of the difference in densities for Rh and Rh₂O₃, distribution (B) is derived for the reduced Rh phase. This now yields an effective average metallic particle diameter of 13 Å. This value now similar to that expected on the basis of the observed co-ordination number in this reduced case (i.e., 7, Table 1). Again, assuming a hemispherical morphology this would imply an average metallic Rh particle diameter of about 11 Å.^[41] Distribution (C) corresponds to the particles that would remain after 40% of the Rh atoms are removed, (vis à vis Figure 9, as Rh(CO)₂). Only particles above 25 Å in diameter are now found to remain once this correction is made.

Discussion

By using EDE, an interrogation of a wide range of the structure-reactive parameter space may be achieved. In the current example, and as with other readily dissociable oxidants,^[18,19,44] supported Rh nanoparticles undergo rapid and extensive oxidation at room temperature. This contrasts starkly with the behaviour of extended Rh surfaces which may be oxidised but only relatively slowly and at temperatures in excess of 500 K.^[2,3] The overall pattern of this oxidation using oxygen is similar to that observed by using H₂S^[43] in that two clearly defined stages are observed.

The simplest rationale for this behaviour under O₂, and one that has been postulated on the basis of previous scanning EXAFS,^[33,34] is that the external region of the particles oxidise very rapidly. This results in formation of a thin layer of oxide surrounding a metallic core. This oxide layer forms a barrier to subsequent oxidation that may only proceed through migration of dissociated oxygen through it and so the metallic core is only subject to relatively slow oxidation. The resulting oxide, even in the “fresh sample” where it is fully formed, is readily reduced by H₂ at room temperature. In this respect the nanoparticulate Rh₂O₃ is very different from the oxidised phases realised through reactive adsorption of NO^[18] and H₂S;^[44] the latter is stable under H₂ to > 673 K, the former only collapsing under H₂ to yield metallic Rh at about 400 K.

This rapid and extensive oxidation process indicates that the phase of the Rh being far from static in the presence of O₂ and CO. As we have previously demonstrated for similar catalysts under NO/H₂ feedstocks,^[19] such an intrinsic reactivity means that the physical state of the Rh component will arise from dynamic redox equilibria. These measurements support this is for CO oxidation catalysis but also indicate a further equilibrium that becomes increasingly important as the CO/O₂ ratio ≥ 1:1. A full understanding of the catalytic oxidation of CO by O₂ over such catalysts, therefore, requires the delineation of two equilibria that occur at the nano scale that is (1) and (2).



Fully reduced nanoparticulate Rh is only achieved and maintained within a relatively small portion of the total reactive parameter space investigated (i.e., temperatures > 450 K and CO/O₂ ratio > 1). So models derived for the description of this catalytic conversion based upon the fundamental chemistry of extended Rh surfaces are only likely to be valid within these conditions. Importantly, in the commercially most relevant arena of a lean feedstock, the active catalytic phase far more resembles nanoparticulate Rh₂O₃ than an extended Rh surface. In these latter situations, CO removal is considerably more efficient (in terms of light off temperature) than in reducing environments.

Surface science based models of CO oxidation utilising Rh single crystals or foils interpret this behaviour in terms of the behaviour of CO and O adsorbed on extended Rh surfaces.^[4–15] At high CO fractions light off is determined by the desorption characteristics of molecularly adsorbed CO; light off only occurs when the rate of CO desorption has become sufficiently advanced that significant levels of oxygen can be dissociated on the CO free portion of the surface. However, even for feedstocks containing a large CO component the current results indicate that, at temperatures up to about 450 K, this is only partly valid in a highly dispersed system, since a considerable portion of the Rh present exists as Rh^I(CO)₂ species. Despite the presence of a high proportion of these Rh^I(CO)₂ species, a net conversion of about 40% is still achieved at 448 K. However, conversions of 80% and 97% are reached at the same temperature when the CO/O₂ ratio is decreased from 2.5:1 to 2:1 or 1.5:1, respectively, and EDE shows the clear formation and maintenance of metallic Rh at and above these temperatures.

The full expression of CO conversion in progressively reducing environments is therefore highly dependent on equilibrium (1) as well as having a component due to the surface chemistry of *fcc*-Rh. It is only when equilibrium (1) is shifted far enough to the left, by increasing temperature or decreasing the CO content of the feed, that we observe the predominant formation of metallic Rh and the concurrent attainment of maximum CO conversion. However, lowering the CO partial pressure within the feedstock also shifts equilibrium (2) to the left and, as a result a progressively oxidised Rh^{III} phase dominates. This latter phase reacts relatively easily with CO and the evidence supplied from probing the variation in EXAFS along the catalyst bed would seem to indicate that the catalytic activity of this phase is derived from a Mars Van Krevelen redox mechanism,^[45] similar to that recently elucidated for the same conversion over thin RuO₂ films.^[46] In this scenario a small Rh core is surrounded oxide at whose surface catalysis is mediated. Moreover, these XANES measurements would suggest that most of the reactive chemistry in this case is occurring within the first millimetre of the bed; thereafter the XANES from the rest of the bed is essentially identical to that observed from the “fresh”, Rh samples that are completely oxidised.

The observation of reactivity in such an oxidised Rh phase provides a structural rationalisation of previous results derived from infra red measurements made during CO oxidation catalysis over similar supported Rh samples.^[29–32] These studies have shown the existence of a CO species that cannot be associated with metallic Rh and whose presence/absence correlates well with oxidation activity. This active species has been associated with CO adsorbed at oxidised Rh centres. Whilst the explicit oxidation state of the Rh is still elusive our results suggest that this IR absorption may be associated with a defective nanoscale Rh oxide phase. The situation shown in Figure 6, wherein metallic Rh is seen to evolve only to be replaced by a phase wherein a metallic core is surrounded by an oxide, also mirrors well the behaviour of similar Rh catalysts observed in this previous IR study.^[32] The appearance of a linear CO band, that we may associate with CO adsorbed upon metallic particles, was also seen to appear and then disappear only to be replaced by CO associated with oxidised Rh sites.

Under net reducing conditions the co-existence of Rh nanoparticles with substantial amounts of $\text{Rh}^{\text{I}}(\text{CO})_2$ is important. Previous scanning EXAFS studies^[21,24] have shown that the oxidative disruption of Rh nanoparticles by CO alone, to yield $\text{Rh}^{\text{I}}(\text{CO})_2$ species, is limited to very small particles; Rh particles showing a Rh–Rh co-ordination of more than four show no propensity for this change in phase. Very recent time resolved studies of this reaction have shown that alumina supported Rh nanoparticles containing about 12–15 atoms (ca. 8 Å diameter) disintegrate rapidly (within ~4 s) to yield this species.^[47] The particles present in our catalysts are considerably larger. Moreover, we have previously shown that supported Rh nanoparticles of the type studied here show no propensity for oxidative disruption under CO alone.^[18] In the current case, we have estimated (Figure 10) that, under the reducing reaction conditions depicted in Figure 7, only Rh particles of greater than 25 Å in diameter still reside in a metallic state.

The explanation for this would seem to be that, under CO alone and at room temperature, this process driven largely by molecular rather than dissociative adsorption. Only a limited amount of energy is derived through molecular adsorption and only enough to overcome the cohesive energy of very small Rh particles and permit the corrosion of the metal particles. The formation of substantial amounts of the $\text{Rh}^{\text{I}}(\text{CO})_2$ under CO rich environments indicates that exothermic O_2 dissociation may be the source of this considerable promotion of the oxidative disruption of supported Rh. Though occurring with a relatively low cross section, CO dissociation over model supported Rh particles has also been observed^[48,49] and therefore may also contribute.

As such CO oxidation over nanoparticulate Rh is far from the simple and structure independent reaction.^[6,7] Even those studies that have shown that traditional structure sensitivities may arise under certain circumstances during this reaction over Rh single crystals,^[14,15] do not yield a complete picture of how this conversion is mediated by nanoscale Rh entities. However, some of these studies have

produced impressive kinetic correlations^[7] between such model and “real” Rh catalysts; moreover, other work on high area supported systems has indicated no appreciable structural sensitivity exists for this conversion.^[17,50] Our work suggests that this is highly improbable for genuinely highly dispersed systems and particularly in the important regime of a highly oxidising feedstock. This apparently contradictory situation may be resolved through consideration of details provided in these previous reports^[7,17,50] regarding the preparation of the high area catalyst used in these previous studies. In these catalysts the Rh was impregnated into 3.3 mm $\gamma\text{-Al}_2\text{O}_3$ (total surface area $110\text{ m}^2\text{ g}^{-1}$) beads. A uniform distribution of the Rh throughout the bead however was not achieved. Instead the Rh only coated the exterior of the bead to a depth of about 30–60 μm . Hence the Rh was constrained to about $0.5\text{--}1\text{ m}^2\text{ g}^{-1}$ rather than over the total $110\text{ m}^2\text{ g}^{-1}$. Moreover, the calcination and reduction conditions used to prepare these catalysts were more extreme (773 K for 4 h in each case^[7,17,50]). The combination of these factors would firstly, lead to a considerable increase in the local loading of the Rh, making the quoted Rh loadings as a poor guide to the final state of the catalyst. Secondly, this situation will lead to the formation of considerably increased Rh particle size for any given loading; this is indeed found to be the case given the TEM results reported here compared to those reported for these previous studies.^[50] The catalysts used in these previous investigations have therefore been made to resemble the low dispersion limit.

Conclusion

CO oxidation over nanoparticulate Rh is a highly structure sensitive reaction. However its structure sensitivity does not arise from differences in surface chemistry of differing low index *fcc*-Rh surfaces. Instead the structure sensitivity we have observed involves the formation and interplay of three structurally discrete supported Rh phases; nanoparticulate Rh, a nanoparticulate Rh_2O_3 like phase, and monodisperse $\text{Rh}^{\text{I}}(\text{CO})_2$ species.

Experimental Section

Sample preparation: 5 wt% Rh/ $\gamma\text{-Al}_2\text{O}_3$ supported samples were prepared through wet impregnation of Al_2O_3 (Degussa Alumina C, surface area ca. $100\text{ m}^2\text{ g}^{-1}$; 1 g) with $\text{RhCl}_3\cdot 3\text{H}_2\text{O}$ (0.13 g) in aqueous solution. This was stirred, using a Teflon-coated magnetic stirrer, for about 1 h until a uniform paste was achieved. The resultant was then dried in an oven overnight. Samples were subsequently sieved through a 120 μm mesh, onto a 90 μm mesh. The fraction retained on the latter was collected and calcined in O_2 at 673 K for 5 h. After cooling to room temperature, the samples were then reduced under a 50% H_2 /He flow at 573 K for 6 h before again being cooled to room temperature under this gas mixture.

Transmission electron microscopy: TEM measurements were recorded in brightfield mode, using reduced (“fresh”) samples, and were carried out on a JEOL FX 2000 microscope.

Energy-dispersive EXAFS (EDE) measurements: 5 wt % Rh/ γ -Al₂O₃ (20 mg) was loaded into a quartz tube (ca. 3.5 mm i.d., wall thickness ca. 0.2 mm) and secured in place using quartz wool plugs. This procedure results in a sample bed about 5 mm in length. The packed tube was then placed into a previously described microreactor,^[37] which allows insertion of a 0.5 mm mineral insulated thermocouple directly into the catalyst bed, sample heating to about 873 K, and the transmission through the sample of the X-ray beam. The exposure of the sample to gas, under mass flow control, is controlled by using three diverter valves. In this configuration, steady flows of individual and mixed gases, as well as gas switching and pulsing can be achieved. Typically a total gas flow of 10 mL min⁻¹ over the sample was utilised to yield gas hourly space velocities (GHSV) of about 10⁴ h⁻¹. The post sample composition of the feedstock was continuously monitored by using a Pfeiffer mass spectrometer station interfaced to the gas flow through a fused silica capillary configured to yield a constant inlet rate to the mass spectrometer. In a typical experiment 16–20 relevant mass fragments are monitored.

The in situ EDE experiments were performed at ID24 at the ESRF, Grenoble, France at the Rh-K edge utilising an asymmetrically cut (6°) Si-[111] monochromator in Laue configuration.^[38] This produces a horizontal beam focus at the sample of about 70–80 μ m and provides, at this energy range, a spread of X-ray energies of about 2.5 keV.^[35] Detection of the X-ray absorption spectra was made using a phosphor-screened, Peltier-cooled, masked CCD camera (Princeton) consisting of 18 stripes of 64 pixel width. Ten of these stripes are summed to form a single spectrum before readout. Currently it is this data readout time that limits the current spectral repetition rate; a spectrum collected by using the sum of 10 strips \times 7 ms exposure and averaged over 10 such acquisitions (i.e., a total acquisition time of 700 ms) yields one spectrum every 3 s.

EDE measurements are made by toggling between the sample bed and a background (I_0) position. Individual spectra can be obtained through a sequential movement between these positions, however, for continuous time resolved acquisition background (I_0) are only made at the beginning and end of the experimental runs to allow continuous monitoring of the sample bed in between times.

Three discrete types of experiment were utilised to build up a picture of the overall behaviour of the Rh catalysts. First, samples were reduced under 5% H₂/He before being purged in He. The gas flow was then switched to 5% O₂/He and the response of the supported Rh phase monitored by using EDE and mass spectrometry. In the second set of experiments samples were again reduced in 5% H₂/He before being purged and then exposed to a reactive gas mixture (derived from flows of 5% CO/He and 5% O₂/He mixed in predetermined proportions) with a total flow of 10 ml min⁻¹. Samples were then heated at 10 K min⁻¹ to 673 K whilst the developing system was monitored in the centre of the catalyst bed. Lastly samples were prepared as for the previous variable temperature experiments and then heated to predetermined temperatures under the reactive feed. EDE measurements were then made sequentially at 200 μ m intervals along the length of the catalyst bed to build up a spatial picture of how the Rh phase present varies as a function of the integral conversion measured by mass spectrometry.

Data handling and analysis: Calibration of the energetic window provided by the bent monochromator was made using a Rh foil maintained within the microreactor setup; calibration files were taken at the beginning and end of each experimental run. Data reduction was carried out using PAXAS^[39] and analysis was made using a spherical wave formalism using EXCURVE98.^[40] “ R factors” quoted are defined as $R = (\int [\chi^T - \chi^E] k^n dk / \int [\chi^E] k^n dk) \times 100\%$ where χ^T and χ^E are the theoretical and experimental EXAFS, k is the photoelectron wavevector, dk is the range of photoelectron wavevectors analysed, and n is the weighting applied to the data.

The room-temperature foil spectra obtained in each run were themselves analysed in EXCURVE98 to check that the energy calibration restored the correct bond lengths (for up to six shells), and reasonable values for their associated Debye Waller (DW) factors and Fermi level (E_f). In these cases the occupancies of up to six shells were defined according to those expected from an ideal fcc (O_h) structure, and analysis for DW fac-

tors, bond lengths and E_f was undertaken using full curved wave multiple scattering theory.

The foil spectra were not, however, utilised to provide a guide to the correct Debye–Waller factors of the supported nanoparticles and their temperature dependence. As the apparent local co-ordination number is intimately convoluted with the magnitude of thermal vibrations of the particles the application of suitable Debye–Waller factors becomes a limiting factor in the accuracy of local co-ordination data, especially in variable temperature studies. Both static and dynamic components of the Debye–Waller factor will be different in a bulk metal and a nanoparticle. Hence the use of a foil to account for the variation in Debye–Waller factor as a function of sample temperature is deemed unsatisfactory. The use of such a bulk system to describe these properties of a nanoparticle will result, at any specific temperature, in an underestimation of the true Debye–Waller factor and therefore an over estimation of the true first shell Rh–Rh co-ordination number (N_1^{Rh}).

In an effort to account for variations in dynamic Debye–Waller factor as a function of temperature samples were heated to 673 K under with H₂. These were then cooled back to room temperature whilst EDE spectra were obtained every 50 K. These spectra were then analysed at each temperature for N_1^{Rh} for range of potential Debye–Waller factors (0.008–0.022). The R factor minimum at each temperature was then used to determine the Debye–Waller factor to be applied analytically at any given temperature. This method is applied with the implicit assumption that that the particle size distribution does not alter as the samples are cooled.

Acknowledgements

The authors would like to thank the ESRF for providing access to their facilities and the EPSRC for funding this research and a post doctoral position to MAN and a studentship to B.J. We are also indebted to: the late Bruce Hancock, John James, Melanie Hill, Ralph Wiegel, and Sebastian Pasternak for their technical expertise. Professor R. Schlögl (Berlin), is also thanked for the generous provision of the mass spectrometer facility available on ID 24.

- [1] J. Koshy, *Thin Solid Films* **1978**, *51*, L17.
- [2] G. L. Kellogg, *J. Catal.* **1985**, *92*, 167.
- [3] A. A. Tolia, R. J. Smiley, W. N. Delglass, C. G. Takoudis, M. J. Weaver, *J. Catal.* **1994**, *150*, 56.
- [4] C. T. Campbell, S.-K. Shi, J. M. White, *J. Phys. Chem.* **1979**, *83*, 225; C. T. Campbell, S.-K. Shi, J. M. White *Appl. Surf. Sci.* **1979**, *2*, 382.
- [5] Y. Kim, J. M. White, *J. Catal.* **1980**, *61*, 374.
- [6] W. M. Daniel, J. M. White, *Int. J. Chem. Kinetics* **1985**, *17*, 413.
- [7] S. H. Oh, G. B. Fisher, J. E. Carpenter, D. W. Goodman, *J. Catal.* **1986**, *100*, 360.
- [8] C. H. F. Peden, D. W. Goodman, S. D. Blair, P. J. Berlowitz, G. B. Fisher, S. H. Oh, *J. Phys. Chem.* **1988**, *92*, 1563.
- [9] L. S. Brown, S. J. Sibener, *J. Chem. Phys.* **1988**, *89*, 1163; L. S. Brown, S. J. Sibener, *J. Chem. Phys.* **1989**, *90*, 2807.
- [10] L.-W. H. Leung, D. W. Goodman, *Catal. Lett.* **1990**, *5*, 353.
- [11] M. Bowker, Q. Guo, R. W. Joyner, *Surf. Sci.* **1993**, *280*, 50.
- [12] F. M. Leible, P. W. Murray, S. M. Francis, G. Thornton, M. Bowker, *Nature* **1993**, *363*, 706.
- [13] D. W. Goodman, C. H. F. Peden, G. B. Fisher, S. H. Oh, *Catal. Lett.* **1993**, *22*, 271.
- [14] M. Bowker, Q. Guo, Y. Li, R. W. Joyner, *Catal. Lett.* **1993**, *18*, 119; M. Bowker, Q. Guo, Y. Li, R. W. Joyner, *Catal. Lett.* **1992**, *22*, 275.
- [15] M. J. P. Hopstaken, J. W. Niemantsverdriet, *J. Chem. Phys.* **2000**, *113*, 5457.
- [16] V. P. Zhdanov, B. Kasemo, *Surf. Sci. Rep.* **1997**, *29*, 31.
- [17] S. H. Oh, C. C. Eickel, *J. Catal.* **1991**, *128*, 526.
- [18] T. Campbell, A. J. Dent, S. Diaz-Moreno, J. Evans, S. G. Fiddy, M. A. Newton, S. Turin, *Chem. Commun.* **2002**, 304.

- [19] M. A. Newton, A. J. Dent, S. Diaz-Moreno, S. G. Fiddy, J. Evans, *Angew. Chem.* **2002**, *114*, 2699; *Angew. Chem. Int. Ed.* **2002**, *41*, 2587.
- [20] C. A. Rice, S. D. Worley, C. W. Curtis, J. A. Guin, A. R. Tarrer, *J. Chem. Phys.* **1981**, *74*, 6487.
- [21] A. C. Yang, C. W. Garland, *J. Phys. Chem.* **1957**, *61*, 1504.
- [22] H. F. T. Van't Blik, J. B. A. D. Van Zon, T. Huiziinga, J. C. Vis, D. C. Koningsberger, R. Prins, *J. Phys. Chem.* **1983**, *87*, 2264.
- [23] B. G. Frederick, G. Apai, T. N. Rhodin, *J. Am. Chem. Soc.* **1987**, *109*, 4797.
- [24] P. Basu, D. Panyatov, J. T. Yates, *J. Phys. Chem.* **1987**, *91*, 3133.
- [25] P. Johnston, R. W. Joyner, *J. Chem. Soc. Faraday Trans.* **1993**, *89*, 863.
- [26] J. Evans, B. E. Hayden, F. Mosselmans, A. Murray, *Surf. Sci.* **1992**, *279*, L159; J. Evans, B. E. Hayden, F. Mosselmans, A. Murray, *Surf. Sci.* **1993**, *301*, 61.
- [27] B. E. Hayden, A. King, M. A. Newton, *Surf. Sci.* **1998**, *397*, 306.
- [28] J. Evans, B. E. Hayden, M. A. Newton, *Surf. Sci.* **2000**, *462*, 169.
- [29] J. A. Anderson, *J. Chem. Soc. Faraday Trans.* **1991**, *87*, 3907.
- [30] T. Ioannides, A. M. Estathiou, Z. L. Zhang, X. E. Verykios, *J. Catal.* **1995**, *156*, 265.
- [31] M. Cavers, J. M. Davidson, I. R. Harkness, L. V. C. Rees, G. S. McDougall, *J. Catal.* **1999**, *188*, 426.
- [32] S. H. Oh, J. E. Carpenter, *J. Catal.* **1983**, *80*, 472.
- [33] J. H. A. Martens, R. Prins, H. Zandbergen, D. C. Koningsberger, *J. Phys. Chem.* **1988**, *92*, 1903.
- [34] J. H. A. Martens, R. Prins, D. C. Koningsberger, *J. Phys. Chem.* **1989**, *93*, 3179.
- [35] M. A. Newton, A. J. Dent, J. Evans, *Chem. Soc. Rev.* **2002**, *31*, 83.
- [36] For instance: a) J. Pellier-Porres, A. Segura, Ch. Ferrer, V. Munoz, A. San Miguel, A. Polian, J. P. Itie, M. Gaultier, S. Pascarelli, *Phys. Rev. B* **2002**, *65*, 174103. b) S. Pascarelli, G. Aquilanti, W. Crichton, L. LeBihan, S. DePanfilis, E. Fabiani, J. Mezouat, J. P. Itie, A. Polian, *High Pres. Res.* **2002**, *22*, 331.
- [37] S. G. Fiddy, M. A. Newton, A. J. Dent, G. Salvini, J. M. Corker, S. Turin, T. Campbell, J. Evans, *Chem. Commun.* **1999**, 851.
- [38] M. Hagelstein, C. Ferraro, U. Hatje, T. Ressler, W. Metz, *J. Synchrotron Radiat.* **1995**, *2*, 174.
- [39] N. Binsted, "PAXAS: Programme for the analysis of X-ray adsorption spectra", University of Southampton, **1988**.
- [40] N. Binsted, EXCURV98, CCLRC Daresbury Laboratory computer programme, **1998**.
- [41] A. Jentys, *Phys. Chem. Chem. Phys.* **1999**, *1*, 4059.
- [42] M. A. Newton, D. G. Burnaby, A. J. Dent, S. Diaz-Moreno, J. Evans, S. G. Fiddy, T. Neisius, S. Pascarelli, S. Turin, *J. Phys. Chem. A* **2001**, *105*, 5965.
- [43] M. A. Newton, D. G. Burnaby, A. J. Dent, S. Diaz-Moreno, J. Evans, S. G. Fiddy, T. Neisius, S. Turin, *J. Phys. Chem. B* **2002**, *106*, 4214.
- [44] M. A. Newton, A. J. Dent, S. Diaz-Moreno, S. G. Fiddy, B. Jyoti, J. Evans, *Chem. Commun.* **2003**, 1906.
- [45] P. Mars, D. W. Van Krevelen, *Chem. Eng. Sci.* **1954**, *3*, 41.
- [46] H. Over, Y. D. Kim, A. P. Seitsonen, S. Wendt, E. Lundgren, M. Schmid, P. Varga, A. Morgante, G. Ertl, *Science* **2000**, *287*, 1474.
- [47] A. Suzuki, Y. Inada, A. Yamaguchi, T. Chihara, M. Yuasa, M. Nomura, Y. Iwasawa, *Angew. Chem.* **2003**, *115*, 4943; *Angew. Chem. Int. Ed.* **2003**, *42*, 4795.
- [48] S. Andersson, M. Frank, A. Sandell, A. Giertz, B. Brena, P. A. Bruwiler, N. Martensson, J. Libuda, M. Baumer, H. J. Freund, *J. Chem. Phys.* **1998**, *108*, 2967.
- [49] A. Berko, T. Biro, F. Solymosi, *J. Phys. Chem.* **2000**, *104*, 2506.
- [50] S. H. Oh, C. C. Eickel, *J. Catal.* **1988**, *112*, 543.

Received: June 6, 2005

Revised: September 2, 2005

Published online: January 10, 2006